Loop effects and nondecoupling property of supersymmetric QCD in $gb \to tH^-$

Guangping Gao

Physics Department, Henan Normal University, Xinxiang 453002, China
and Institute of Theoretical Physics, Academia Sinica, Beijing 100080, China

Gongru Lu

Physics Department, Henan Normal University, Xinxiang 453002, China

Zhaohua Xiong

CCAST (World Laboratory), P.O. Box 8730, Beijing 100080, China
and Institute of High Energy Physics, Academia Sinica, Beijing 100039, China

Jin Min Yang

Institute of Theoretical Physics, Academia Sinica, Beijing 100080, China

The one-loop supersymmetric (SUSY) QCD radiative correction to the $gb \to tH^-$ cross section is calculated in the minimal supersymmetric standard model. We find that SUSY QCD is nondecoupling if the gluino mass and the parameters μ, A_t, and A_b are of the same order and get large. The nondecoupling contribution can be enhanced by large $\tan\beta$ and therefore large corrections to the hadronic production rates at the Fermilab Tevatron and CERN Large Hadron Collider (LHC) are expected in the large $\tan\beta$ limit. The fundamental reason for such nondecoupling behavior is that some couplings in the loops are proportional to the SUSY mass parameters.

I. INTRODUCTION

Although the standard model (SM) is phenomenologically successful, it is arguably an effective theory and new physics must exist at high energy scales. Among the elementary particles predicted by the SM, the top quark and Higgs boson may hold the key to new physics since they are most related to electroweak symmetry breaking. An intensive study of the properties of the top quark and Higgs boson will be one of the primary tasks of particle physics in the new millennium.

So far the most intensively studied new physics model is the minimal supersymmetric standard model (MSSM) [1]. This model predicts the existence of five Higgs bosons H^0, h^0, A^0, and $H^\pm$, all of which couple to the top quark. Compared to the couplings in the SM, the coupling tbH^- is a completely new coupling. Studies [2] show that this coupling is sensitive to quantum corrections and may be a good probe of the MSSM. Although this coupling could be measured from the top quark decay process $t \to H^+ b$ if the charged Higgs boson is sufficiently light, the direct production of a top quark associated with the charged Higgs boson through the subprocess $gb \to tH^-$ at hadron colliders will be a good probe for tbH^- coupling [3,4]. In this work we calculate the one-loop supersymmetric (SUSY) QCD corrections to this process with the following motivations. First, if the charged Higgs boson is heavy, $m_{H^+} > m_t + m_b$, as a main H^+ production channel [5], the process $gb \to tH^-$ will provide a sizable cross section at the Fermilab Tevatron and CERN Large Hadron Collider (LHC). The supersymmetric radiative corrections, especially the SUSY QCD corrections, to this high energy process may be significant, as was found for other similar processes [6–10]. Second, some recent studies

[8–10] showed that SUSY QCD may be nondecoupling in some processes involving Higgs bosons. As is well known, the decoupling theorem [11] states that, under certain conditions in a given quantum field theory with light and heavy particles, if the heavy particles are integrated out to all orders in perturbation theory, the remaining effective action that is valid at energies much lower than the heavy particle masses does not show any trace of these heavy particles. If SUSY QCD is nondecoupling in some cases, we need a proper understanding and thus we need to further investigate this nondecoupling property of SUSY QCD. $gb \to tH^-$ is an ideal process for this purpose.

This paper is organized as follows. In Sec. II we present the formula for the one-loop SUSY QCD corrections to the $gb \to tH^-$ process. In Sec. III we scan the parameter space of the MSSM to estimate the size of SUSY QCD corrections. In Sec. IV we study the decoupling behavior of SUSY QCD. A discussion of how the decoupling and nondecoupling take place is also given. Finally, the conclusions are summarized in Sec. V.

II. CALCULATIONS

The subprocess $gb \to tH^-$ occurs through both s channel and t channel. The tree-level amplitude is given by

$$M_0 = M_0^{(s)} + M_0^{(t)}, \tag{2.1}$$

where $M_0^{(s)}$ and $M_0^{(t)}$ represent the amplitudes arising from the s-channel diagram shown in Fig. 1(a) and the t-channel diagram shown in Fig. 1(b), respectively. Their amplitudes can be expressed as
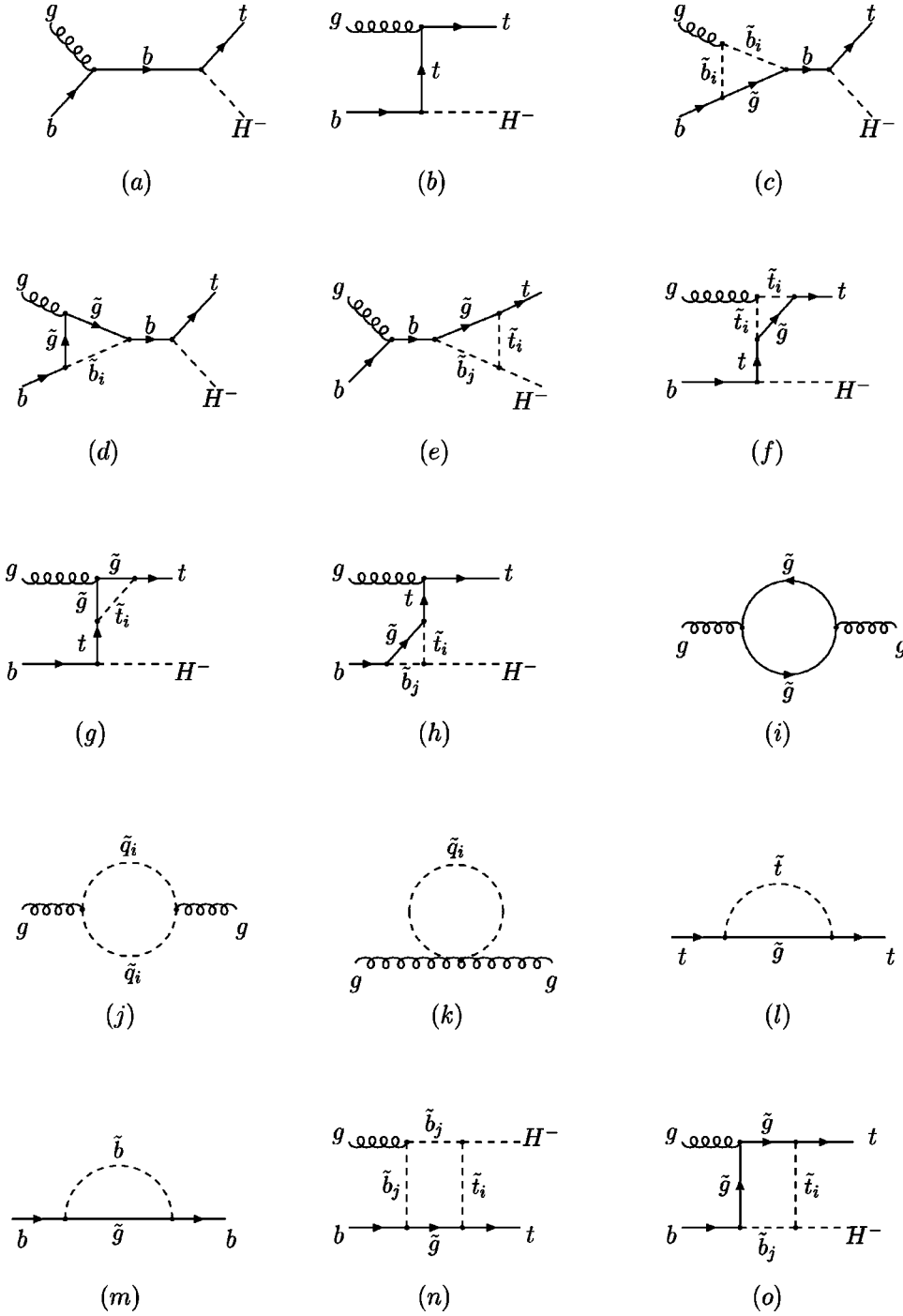
FIG. 1. Feynman diagrams of $gb \rightarrow tH^-$ with one-loop SUSY QCD corrections: (a) and (b) are tree-level diagrams; (c)–(e) are one-loop vertex diagrams for the s channel; (f)–(h) are one-loop vertex diagrams for the t channel; (i)–(m) are self-energy diagrams; (n),(o) are box diagrams.

$$M_0^{(s)} = \frac{ig g_s V_{tb}}{\sqrt{2} m_W (\hat{s} - m_b^2)} \bar{u}(p_t)[2\eta_t p_b^\mu P_L + 2\eta_b p_b^\mu P_R - \eta_t \gamma^\mu \not{k} P_L - \eta_b \gamma^\mu \not{k} P_R] u(p_b) \varepsilon_\mu(k) T_{ij}^a, \qquad (2.2)$$

$$M_0^{(t)} = \frac{ig g_s V_{tb}}{\sqrt{2} m_W (\hat{t} - m_t^2)} \bar{u}(p_t)[2\eta_t p_t^\mu P_L + 2\eta_b p_t^\mu P_R - \eta_t \gamma^\mu \not{k} P_L - \eta_b \gamma^\mu \not{k} P_R] u(p_b) \varepsilon_\mu(k) T_{ij}^a, \qquad (2.3)$$

where $P_{R,L} \equiv (1 \pm \gamma_5)/2$, and p_t, p_b, and k are the momenta of the outgoing top quark, the incoming bottom quark, and the incoming gluon, respectively. $\hat{s}$ and $\hat{t}$ are the subprocess Mandelstam variables defined by $\hat{s} = (p_b + k)^2 = (p_t + p_{H^-})^2$ and $\hat{t} = (p_t - k)^2 = (p_{H^-} - p_b)^2$. T^a are the SU(3) color matrices and $\tan\beta = v_2/v_1$ is the ratio of the vacuum expectation values of the two Higgs doublets. The constants $\eta_{b,t}$ are defined by $\eta_b = m_b \tan\beta$ and $\eta_t = m_t \cot\beta$.

The one-loop Feynman diagrams of SUSY QCD corrections are shown in Figs. 1(c)–1(o). In our calculations we use dimensional regularization to control all the ultraviolet divergences in the virtual loop corrections and we adopt the on-mass-shell renormalization scheme. The renormalization condition for the coupling constant g_s is similar to that for the coupling constant e in QED, i.e., the coupling of the photon (gluon) to a pair of fermions is required to recover the tree-level result in the limit of zero momentum transfer. This condition yields

$$\frac{\delta g_s}{g_s} = -\frac{1}{2}\delta Z_2^g, \tag{2.4}$$

where δg_s and Z_2^g are the renormalization constants defined by $g_s^0 \equiv g_s + \delta g_s$ and $A_\mu^0 \equiv \sqrt{Z_2^g} A_\mu$ with g_s^0 denoting the bare coupling constant and A_μ^0 bare gluon fields (color index suppressed).

Including the one-loop SUSY QCD corrections, the renormalized amplitude for $gb \to tH^-$ can be written as

$$M_{ren} = M_0^{(s)} + M_0^{(t)} + \delta M, \tag{2.5}$$

where δM represents the one-loop SUSY QCD corrections given by

$$\delta M = \delta M^{V_1(s)} + \delta M^{V_2(s)} + \delta M^{s(s)} + \delta M^{box} + \delta M^{V_1(t)} + \delta M^{V_2(t)} + \delta M^{s(t)}. \tag{2.6}$$

Here $\delta M^{V_1(s)}$, $\delta M^{V_2(s)}$, and $\delta M^{s(s)}$ represent the renormalized vertices $gb\bar{b}$ and $t\bar{b}H^-$, and the renormalized propagator in the s-channel diagram, respectively. Similar definitions exist for $\delta M^{V_1(t)}$, $\delta M^{V_2(t)}$, and $\delta M^{s(t)}$ in the t-channel diagram. The contribution of the box diagram is denoted by δM^{box}. Each δM^l can be decomposed as

$$\delta M^l = \frac{ig g_s^3 T_{ij}^a V_{tb}}{16\sqrt{2}\pi^2 m_W} C^l \bar{u}(p_t)\{F_1^l \gamma^\mu P_L + F_2^l \gamma^\mu P_R + F_3^l p_b^\mu P_L + F_4^l p_b^\mu P_R + F_5^l p_t^\mu P_L + F_6^l p_t^\mu P_R + F_7^l \gamma^\mu \not{k} P_L + F_8^l \gamma^\mu \not{k} P_R + F_9^l p_b^\mu \not{k} P_L$$

$$+ F_{10}^l p_b^\mu \not{k} P_R + F_{11}^l p_t^\mu \not{k} P_L + F_{12}^l p_t^\mu \not{k} P_R\}u(p_b)\varepsilon_\mu(k), \tag{2.7}$$

where the coefficients C^l and the form factors F_n^l are given explicitly in Appendixes A and B, respectively. We have checked that all the ultraviolet divergences cancel as a result of the renormalizability of the MSSM.

The amplitude squared is given by

$$\overline{\sum} |M_{ren}|^2 = \overline{\sum} |M_0^{(s)} + M_0^{(t)}|^2 + 2\,\text{Re}\overline{\sum} [(M_0^{(s)} + M_0^{(t)})^\dagger \delta M], \tag{2.8}$$

where

$$\overline{\sum} |M_0^{(s)} + M_0^{(t)}|^2 = \frac{2g^2 g_s^2 |V_{tb}|^2}{N_C m_W^2}\left\{ \frac{1}{(\hat{s}-m_b^2)^2}[(\eta_b^2 + \eta_t^2)(p_b \cdot k p_t \cdot k + 2p_b \cdot k p_b \cdot p_t - m_b^2 p_t \cdot k - m_b^2 p_b \cdot p_t) \right.$$

$$+ 2m_b^2 m_t^2(p_b \cdot k - m_b^2)] + \frac{1}{(\hat{t}-m_t^2)^2}[(\eta_b^2 + \eta_t^2)(p_b \cdot k p_t \cdot k + m_t^2 p_b \cdot k - m_t^2 p_b \cdot p_t) + 2m_b^2 m_t^2(p_t \cdot k$$

$$- m_t^2)] + \frac{1}{(\hat{s}-m_b^2)(\hat{t}-m_t^2)}[(\eta_b^2 + \eta_t^2)(2p_b \cdot k p_t \cdot k + 2p_b \cdot k p_b \cdot p_t - 2(p_b \cdot p_t)^2 - m_b^2 p_t \cdot k + m_t^2 p_b \cdot k)$$

$$\left. + 2m_b^2 m_t^2(p_t \cdot k - p_b \cdot k - 2p_b \cdot p_t)] \right\}, \tag{2.9}$$

$$\overline{\sum} (M_0^{(s)} + M_0^{(t)})^\dagger \delta M = -\frac{g^2 g_s^4 |V_{tb}|^2}{64 N_C \pi^2 m_W^2} \sum_{n=1}^{12}\left[\frac{1}{\hat{s}-m_b^2}h_n^{(s)} + \frac{1}{\hat{t}-m_t^2}h_n^{(t)}\right]C^l F_n^l. \tag{2.10}$$

Here the color factor $N_C = 3$, and $h_n^{(s)}$ and $h_n^{(t)}$ can be found in Appendix A.

The cross section for the parton process $gb \to tH^-$ is

$$\hat{\sigma}(\hat{s}) = \int_{\hat{t}_{min}}^{\hat{t}_{max}} \frac{1}{16\pi\hat{s}^2}\overline{\sum}|M_{ren}|^2 d\hat{t}, \tag{2.11}$$

with

$$\hat{t}_{max,min} = \frac{1}{2}\{m_t^2 + m_{H^-}^2 - \hat{s}$$

$$\pm \sqrt{[\hat{s}-(m_t+m_{H^-})^2][\hat{s}-(m_t-m_{H^-})^2]}\}. \tag{2.12}$$

The total hadronic cross section for pp(or $p\bar{p}$)$\rightarrow tH^-$ $+X$ can be obtained by folding the subprocess cross section $\hat{\sigma}$ with the parton luminosity:

$$\sigma(s) = \int_{\tau_0}^{1} d\tau \frac{dL}{d\tau} \hat{\sigma}(\hat{s} = s\tau), \qquad (2.13)$$

where $\tau_0 = (m_t + m_{H^-})^2/s$, and s is the pp(or $p\bar{p}$) center-of-mass energy squared. $dL/d\tau$ is the parton luminosity given by

$$\frac{dL}{d\tau} = \int_{\tau}^{1} \frac{dx}{x} [f_g^p(x,Q) f_b^p(\tau/x,Q) + (g \leftrightarrow b)], \quad (2.14)$$

where f_b^p and f_g^p are the bottom quark and gluon distribution functions in a proton, respectively. In our numerical calculation, we use the CTEQ5L parton distribution functions [12] with $Q = m_t + m_{H^-}$.

To show the size of the corrections, we define the relative quantity

$$\Delta_{SQCD} = \frac{\sigma - \sigma_0}{\sigma_0}, \qquad (2.15)$$

where σ_0 is the tree-level cross section.

III. NUMERICAL RESULTS

Before performing numerical calculations, we take a look at the relevant parameters involved.

For the SM parameters, we took $m_W = 80.448$ GeV, $m_Z = 91.187$ GeV, $m_t = 176$ GeV, $m_b = 4.5$ GeV, and used the two-loop running coupling constant $\alpha_s(Q)$.

For the SUSY parameters, apart from the charged Higgs boson mass, gluino mass, and $\tan\beta$, the mass parameters of top and bottom squarks are involved. The mass-square matrices of top and bottom squarks take the form ($q = t$ or b) [13]

$$M_{\tilde{q}}^2 = \begin{pmatrix} m_{\tilde{q}_L}^2 & m_q X_q^\dagger \\ m_q X_q & m_{\tilde{q}_R}^2 \end{pmatrix}, \qquad (3.1)$$

where

$$m_{\tilde{q}_L}^2 = m_{\tilde{Q}}^2 + m_q^2 - m_Z^2 \left(\frac{1}{2} + e_q \sin^2\theta_W \right) \cos(2\beta),$$

$$m_{\tilde{q}_R}^2 = m_{\tilde{U},\tilde{D}}^2 + m_q^2 + e_q m_Z^2 \sin^2\theta_W \cos(2\beta), \qquad (3.2)$$

$$X_q = \begin{cases} A_t - \mu \cot\beta & \text{for } q = t, \\ A_b - \mu \tan\beta & \text{for } q = b. \end{cases}$$

Here $m_{\tilde{Q}}^2$, $m_{\tilde{U}}^2$, and $m_{\tilde{D}}^2$ are soft-breaking mass terms for the left-handed squark doublet $\tilde{Q}$, right-handed up squark $\tilde{U}$, and down squark $\tilde{D}$, respectively. A_b (A_t) is the coefficient of the

trilinear term $H_1 \tilde{Q} \tilde{D}$ ($H_2 \tilde{Q} \tilde{U}$) in soft-breaking terms and μ is the bilinear coupling of the two Higgs doublet in the superpotential. Thus the SUSY parameters involved in top and bottom squark mass matrices are

$$m_{\tilde{Q}}, m_{\tilde{U}}, m_{\tilde{D}}, A_t, A_b, \mu, \tan\beta.$$

The mass-square matrices are diagonalized by unitary rotations ($q = t$ or b)

$$R^q = \begin{pmatrix} \cos\theta_q & \sin\theta_q \\ -\sin\theta_q & \cos\theta_q \end{pmatrix} \qquad (3.3)$$

which relates the weak eigenstates ($\tilde{q}_L, \tilde{q}_R$) to the mass eigenstates ($\tilde{q}_1, \tilde{q}_2$). Then the top and bottom squark masses as well as the mixing angles are obtained by

$$m_{\tilde{q}_{1,2}} = \frac{1}{2} [m_{\tilde{q}_L}^2 + m_{\tilde{q}_R}^2$$
$$\pm \sqrt{(m_{\tilde{q}_L}^2 - m_{\tilde{q}_R}^2)^2 + 4 m_q^2 X_q^2}], \qquad (3.4)$$

$$\tan 2\theta_q = \frac{2 m_q X_q}{m_{\tilde{q}_L}^2 - m_{\tilde{q}_R}^2}.$$

To determine the mixing angles completely, we adopt the convention in [14] which sets $\theta_q = \pi/4$ if $m_{\tilde{q}_L} = m_{\tilde{q}_R}$ and shifts $\pi/2$ to θ_q if $m_{\tilde{q}_L} > m_{\tilde{q}_R}$. Thus θ_q lies in the range $-\pi/4 \le \theta_q \le \frac{3}{4}\pi$.

To find the size of the one-loop SUSY QCD effects, we performed a scan over the nine-dimensional parameter space $m_{\tilde{Q}}$, $m_{\tilde{U}}$, $m_{\tilde{D}}$, A_t, A_b, μ, $\tan\beta$, m_{H^-}, $m_{\tilde{g}}$. In scanning we restricted m_{H^-}, A_t, A_b, and μ to the sub-TeV region and required $m_{H^-} > 150$ GeV. Other mass parameters are assumed to be smaller than 5 TeV. In addition, we consider the following experimental constraints: (1) $\mu > 0$ and a large $\tan\beta$ in the range $5 \le \tan\beta \le 50$, which might be favored by the recent muon $g-2$ measurement [15]. (2) The CERN $e^+ E^-$ LEP and Collider Detector at Fermilab (CDF) lower mass bounds on gluino, top and bottom squark [16]

$$m_{\tilde{t}_1} \ge 86.4 \text{ GeV}, \quad m_{\tilde{b}_1} \ge 75.0 \text{ GeV}, \quad m_{\tilde{g}} \ge 190 \text{ GeV}. \qquad (3.5)$$

The scan results are plotted in the plane of Δ_{SQCD} versus θ_b in Fig. 2.

From Fig. 2 one can see that in most parameter space the mixing of bottom squarks is small while the one-loop SUSY QCD effect can be quite large. In some part of the parameter space, the correction size can be larger than 20%, which cannot be neglected in the study of this process at the LHC.
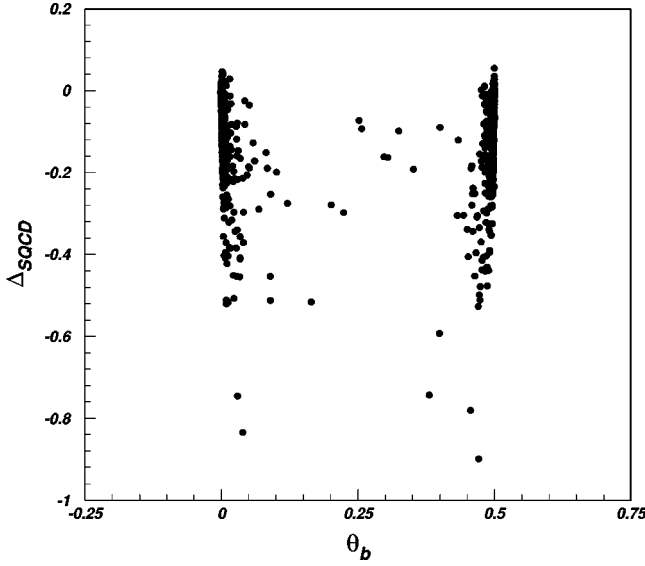
FIG. 2. The scatter plot in the plane of Δ_{SQCD} versus θ_b. The scan was performed over nine SUSY parameters. θ_b is in unit of π.

FIG. 3. Nondecoupling behavior of Δ_{SQCD} with $m_{\tilde{Q}}=m_{\tilde{U}}$ $=m_{\tilde{D}}=m_{\tilde{g}}=A_b=A_t=\mu=m_S$ and for different values of $\tan\beta$. Corrections at the Tevatron with $\sqrt{s}=2$ TeV (solid lines) and at the LHC with $\sqrt{s}=14$ TeV (dashed lines) are plotted.

IV. DECOUPLING PROPERTY OF SUSY QCD

To find out if SUSY QCD is decoupling from the process $gb\rightarrow tH^-$ in the large limit of SUSY mass parameters, we fix the charged Higgs boson mass as $m_{H^-}=250$ GeV and consider the following scenarios.

(1) *Scenario A*. All squark (collectively denoted by m_S) and gluino masses and μ or A parameters are of the same size and much heavier than the electroweak scale, i.e.,

$$m_S\sim m_{\tilde{Q}}\sim m_{\tilde{U}}\sim m_{\tilde{D}}\sim m_{\tilde{g}}$$
$$\sim\mu \text{ or } A_t \text{ or } A_b\gg M_{EW}. \quad (4.1)$$

In this case, mixings in both the bottom and top squark sectors reach their maximal values, i.e., $\theta_t\sim\pm\pi/4$, $\theta_b\sim\pm\pi/4$. As shown in Eqs. (A3)–(A5), the couplings α_{ij} in the vertex $H^-\tilde{t}_i\tilde{b}_j$ are proportional to the linear combination of $\mu+A_b\tan\beta$ and $\mu+A_t\cot\beta$. Considering that the couplings α_{ij} are proportional to m_S as μ or $A_{t,b}$ gets as large as m_S, and the loop scalar integral function C_0 goes to $-1/2m_S^2$ as $m_S\gg\hat{s}$ [see Eq. (C4) in this paper and Eq. (B8) in Ref. [9]], one can infer that the terms $\alpha_{ij}A_{ij}^{2(L,R)}C_0^6m_{\tilde{g}}$ which arise from the vertex correction to H^-tb do not vanish but go to a nonzero constant, showing a clear indication of *nondecoupling* behavior. In fact, such nondecoupling behavior will happen as long as the gluino mass and μ or A parameters are of the same order, not necessarily degenerate. Actually, from the expansions of the three- and four-point loop integrals in the asymptotic large mass limit in Appendix C, one can see this fact.

As illustrative examples, we plot the dependence of the SUSY QCD correction to $gb\rightarrow tH^-$ on the common SUSY parameter m_S in Fig. 3. From this figure one can see that the nondecoupling behavior indeed happens. As for the dependence of the nondecoupling effects on $\tan\beta$, it is quite in-
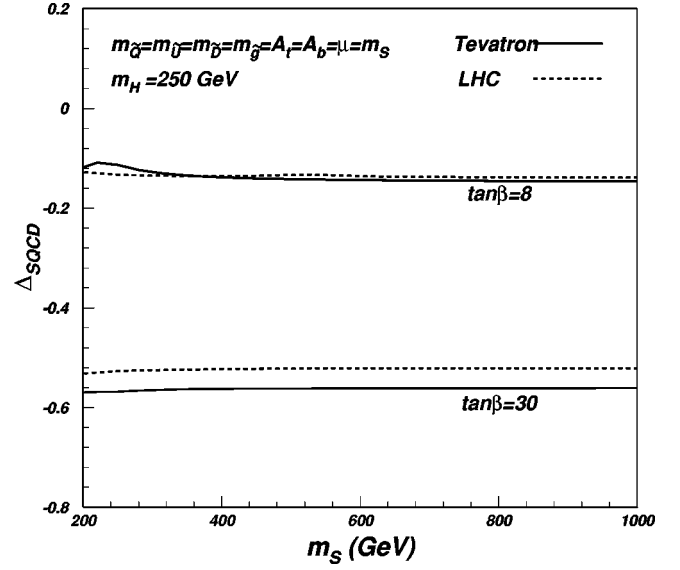
volved and complicated. For the parameter values chosen in our numerical examples, the corrections are enhanced by $\tan\beta$.

(2) *Scenario B*. The gluino mass and μ are of the same order (collectively denoted by m_S) and get much larger than squark masses and the electroweak scale: i.e.,

$$m_S\sim m_{\tilde{g}}\sim\mu\gg m_{\tilde{Q}}\sim m_{\tilde{U}}\sim m_{\tilde{D}}\gg M_{EW}. \quad (4.2)$$

To keep top and bottom squark masses from getting large, we can set $A_t\simeq\mu\cot\beta$, $A_b\simeq\mu\tan\beta$. In this scenario, no mixings occur in the bottom and top squark sectors. Apart from the vertex correction discussed in scenario A, the terms such as $\alpha_{ij}A_{ij}^{2(L,R)}D_0^2m_{\tilde{g}}$ in the box contribution [see Eqs. (B8) and (C10)] do not vanish either since the four-point integral functions $D_{(0,1l)}^2\rightarrow 1/m_{\tilde{g}}^2 (l=1,2,3)$ when $m_{\tilde{g}}^2\gg\hat{s}$. So in this case the SUSY QCD is nondecoupling. This differs from scenario A where $D_{(0,1l)}\rightarrow 1/m_{\tilde{g}}^4$.

Although the nondecoupling effects can arise from more diagrams in this case, the reason is the same as in scenario A; i.e., the couplings $H^-\tilde{t}_i\tilde{b}_j$ are proportional to μ. To prove this point fully, now let us focus our attention on the terms arising from the corrections to the $gb\bar{b}$ and $g\tilde{g}\tilde{g}$ vertices, which are also likely to give contributions to the nondecoupling effects in both scenarios we discussed. First, for example, we consider the term

$$-\frac{2}{3}\eta_t C_{24}^1-3\eta_t[m_{\tilde{g}}^2 C_0^2-2C_{24}^2+1/2]$$

$$+\frac{16\pi^2}{g_s^2}\eta_t 2\delta Z_R^b \quad (4.3)$$

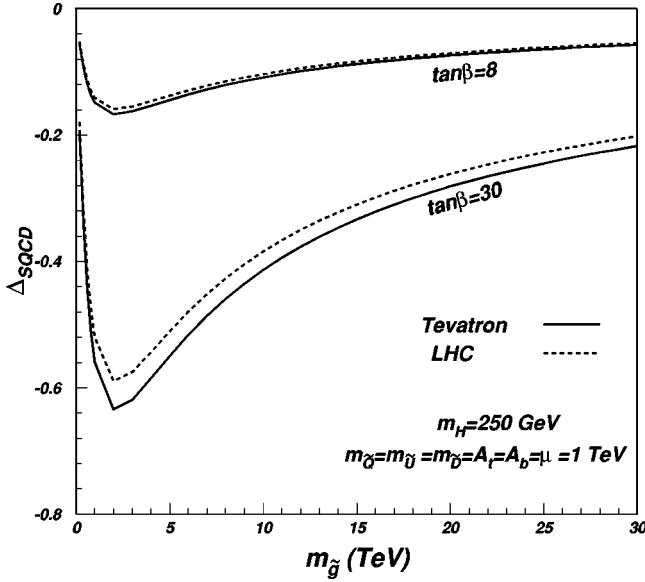FIG. 4. Behavior of Δ_{SQCD} in the large $m_{\tilde{g}}$ limit with fixed $m_{\tilde{Q}}=m_{\tilde{U}}=m_{\tilde{D}}=A_b=A_t=\mu=1$ TeV and for different values of $\tan\beta$. The solid and dashed lines correspond to corrections at the Tevatron with $\sqrt{s}=2$ TeV and at the LHC with $\sqrt{s}=14$ TeV, respectively.

FIG. 5. Behavior of Δ_{SQCD} in the large squark mass limit with fixed $m_{\tilde{g}}=A_b=A_t=\mu=1$ TeV and for different values of $\tan\beta$. The solid and dashed lines correspond to corrections at the Tevatron with $\sqrt{s}=2$ TeV and at the LHC with $\sqrt{s}=14$ TeV, respectively.

in $F_3^{1(s)}$. From Eqs. (B9), (C2), (C4), (C5), (C7), and (C8), we draw the conclusion that the term indeed cancels out. Further, it is easy to find that all terms related to A_{bi}^2 are zero in the asymptotic large mass limit. This is also valid in scenario C and scenario D that we will study. Second, we examine the terms such as $\alpha_{ij}A_{ij}^{1(L,R)}D_0^1 m_{\tilde{g}}^2$ in Eq. (B8). The asymptotic form of the function D_0^1 in the large mass limit is always proportional to $1/m_{\tilde{g}}^4$ and different from D_0^2, which is proportional to $1/m_{\tilde{g}}^2$ in scenario B. So the terms do not cause nondecoupling either.

(3) *Scenario C*. Only the gluino mass is very much larger than other SUSY parameters and the electroweak scale. In this scenario, to simplify the calculation we assumed $m_S=m_{\tilde{Q}}=m_{\tilde{U}}=m_{\tilde{D}}=\mu=A_t=A_b=1$ TeV. As shown in Fig. 4, the SUSY QCD decouples. The reason is that the couplings α_{ij} in the vertex $H^-\tilde{t}_i\tilde{b}_j$ are fixed, and in this case a scalar function such as C_0^6 is proportional to $(1/m_{\tilde{g}}^2)\log(m_S^2/m_{\tilde{g}}^2)[1+\hat{s}/2m_{\tilde{g}}^2]$ when $m_{\tilde{g}}^2\gg\hat{s}$ [see Eqs. (C4),(C12)]; thus the SUSY QCD correction varies as $(1/m_{\tilde{g}}^2)\log(m_S^2/m_{\tilde{g}}^2)$.

In this scenario, since $\hat{s}$ can be up to the large collider beam energy squared s, not only the logarithmic dependence on the large mass parameter but also the large collider beam energies are responsible for the slow decoupling of the gluino, especially at the LHC, as shown in Fig. 4. This is different from the previous studies of various decays [8–10].

(4) *Scenario D*. The squark masses are of the same order (collectively denoted by m_S) and very large compared to other SUSY parameters and the electroweak scale. As shown in Fig. 5, the SUSY QCD also decouples. In this case, it decouples much faster than in scenario C where only the gluino mass gets large. This can be understood easily be-
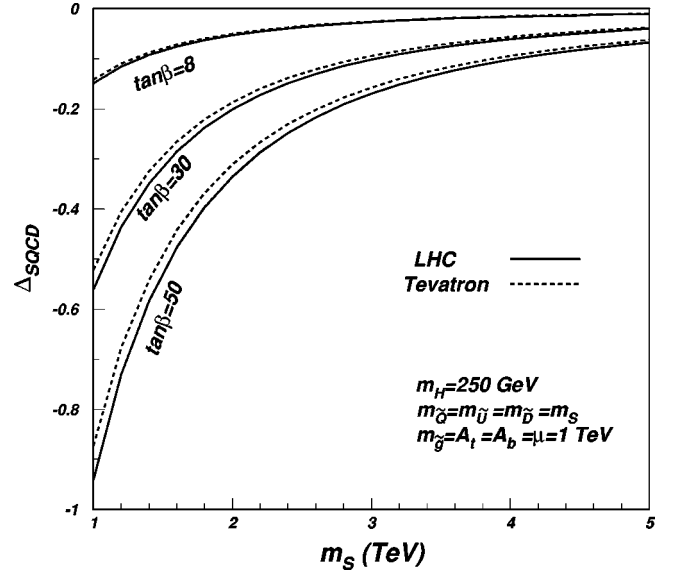
cause in this case the couplings α_{ij} in the vertex $H^-\tilde{t}_i\tilde{b}_j$ and the mass of the gluino are both fixed, so that the SUSY QCD correction varies as $\sim C_{11}^1\rightarrow(1/m_S^2)\log(m_{\tilde{g}}^2/m_S^2)$.

Some remarks on the SUSY QCD correction to the process of $gb\rightarrow tH^-$ are in order.

(1) From the above analysis we find that the fundamental reason for such nondecoupling behavior of SUSY QCD in the process $gb\rightarrow tH^-$ is that some couplings like $H^-\tilde{t}_i\tilde{b}_j$ are proportional to SUSY mass parameters. This is similar to the nondecoupling property of the heavy top quark in the SM, where the top quark Yukawa couplings are proportional to the top quark mass.

(2) The nondecoupling behavior shown in Fig. 3 is in agreement with previous studies of SUSY QCD corrections in some decay processes [8,9]. In particular, the correction Δ_{SQCD} shown in this figure as a function of the common scale m_S and $\tan\beta$ looks quite similar to the corresponding corrections in the partial decay width $\Gamma(H^+\rightarrow t\bar{b})$, as given in Fig. 2 of Ref. [9]. The same kinds of similarities are also found between Fig. 4 here and Fig. 6 of Ref. [9], and between Fig. 5 here and Fig. 7 of Ref. [9]. Although the processes are different, the fundamental reason for such nondecoupling behavior is the same.

(3) From Figs. 3–5 one sees that the size of SUSY QCD corrections can be quite large for large $\tan\beta$. Note that when one-loop effects are too large, higher level loops must also be calculated. We refer the reader to Ref. [17] where some techniques of resummation for better convergence are proposed.

(4) As shown in Ref. [4], the genuine QCD corrections to this process are also sizable, which can enhance the production rate by 40%–80% when the charged Higgs boson mass and $\tan\beta$ vary in the ranges 180–1000 GeV and 2–50, respectively. It is clear that the SUSY QCD corrections evaluated in this work are comparable in size to the genuine QCD

corrections. It is noticeable that the genuine QCD corrections are always positive whereas the SUSY QCD corrections are negative in most SUSY parameter space.

V. CONCLUSIONS

In this work we evaluated SUSY QCD radiative corrections to $gb \rightarrow tH^-$ at the Tevatron and LHC. We found that in some parameter spaces the one-loop SUSY QCD correction can be quite large and cannot be neglected. We discussed in detail the decoupling behavior of the corrections in the large SUSY mass limit, and found that with fixed gluino mass the one-loop SUSY QCD corrections decouple; while nondecoupling occurs when the gluino mass and μ or A parameters both get large. The nondecoupling behavior of the SUSY QCD corrections in the process $gb \rightarrow tH^-$ is similar to the ones found in the literature for the Higgs particle and top quark decays. We pointed out that such nondecoupling behavior arises from the $H^- \tilde{t}_i \tilde{b}_j$ vertices, which are proportional to SUSY mass parameters, as stated in some previous work [8–10]. Such large nondecoupling effects may play an important role in the indirect search for SUSY from the production of a top quark associated with a charged Higgs boson at the Tevatron and LHC.

ACKNOWLEDGMENTS

APPENDIX A

Here we list the coefficients C^l, scalar functions $h_n^{(l)}$, and vertex $V(H^- \tilde{t}_i \tilde{b}_j) = ig\alpha_{ij}/\sqrt{2}m_W$ $(i,j=1,2)$ needed in our calculations.

Coefficients C^l:

$$C^{V(s)} = \frac{1}{\hat{s} - m_b^2}, \quad C^{V(t)} = \frac{1}{\hat{t} - m_t^2},$$

$$C^{s(s)} = \frac{1}{(\hat{s} - m_b^2)^2}, \quad C^{s(t)} = \frac{1}{(\hat{t} - m_t^2)^2}, \tag{A1}$$

$$C^{box} = 1.$$

Scalar functions $h_n^{(l)}$:

$$h_1^{(l)} = 4m_t \eta_t (2p_b \cdot k - p^{(l)} \cdot p_b)$$
$$- 4m_b \eta_b (p^{(l)} \cdot p_t + p_t \cdot k),$$

$$h_3^{(l)} = 2\eta_t (2p_b \cdot k p_b \cdot p_t - m_b^2 p_t \cdot k$$
$$- 2p^{(l)} \cdot p_b p_b \cdot p_t)$$
$$+ 2m_b m_t \eta_b (p_b \cdot k - 2p^{(l)} \cdot p_b),$$

$$h_5^{(l)} = 2\eta_t (m_t^2 p_b \cdot k - 2p^{(l)} \cdot p_t p_b \cdot p_t)$$
$$+ 2m_b m_t \eta_b (p_t \cdot k - 2p^{(l)} \cdot p_t),$$

$$h_7^{(l)} = 4\eta_t (p^{(l)} \cdot p_b p_t \cdot k - p^{(l)} \cdot k p_b \cdot p_t$$
$$- p_b \cdot k p^{(l)} \cdot p_t - 2p_b \cdot k p_t \cdot k)$$
$$- 4m_b m_t \eta_b p^{(l)} \cdot k, \tag{A2}$$

$$h_9^{(l)} = 4m_t \eta_t p_b \cdot k (p_b \cdot k - p^{(l)} \cdot p_b)$$
$$- 4m_b \eta_b p^{(l)} \cdot p_b p_t \cdot k,$$

$$h_{11}^{(l)} = 4m_t \eta_t p_b \cdot k (p_t \cdot k - p^{(l)} \cdot p_t)$$
$$- 4m_b \eta_b p_t \cdot k p^{(l)} \cdot p_t,$$

$$h_{2,4,6,8,10,12}^{(l)} = h_{1,3,5,7,9,11}^{(l)} (\eta_b \leftrightarrow \eta_t),$$

where the index l represents the two channels s and t, and $p^{(s)} = p_b$, $p^{(t)} = p_t$.

Couplings of $H^- \tilde{t}_i \tilde{b}_j$: The $H^- \tilde{t}_i \tilde{b}_j$ interaction terms can be parametrized as

$$\mathcal{L}_{H^- \tilde{t}_i \tilde{b}_j} = \frac{g}{\sqrt{2}m_W} \alpha_{ij} \quad (i,j=1,2), \tag{A3}$$

where

$$\alpha_{ij} = R_{i1}^{t*} R_{j1}^b g_{LL} + R_{i2}^{t*} R_{j2}^b g_{RR} + R_{i1}^{t*} R_{j2}^b g_{LR}$$
$$+ R_{i2}^{t*} R_{j1}^b g_{RL} \tag{A4}$$

with

$$g_{LL} = -m_W^2 \sin 2\beta + m_b^2 \tan \beta + m_t^2 \cot \beta,$$

$$g_{RR} = m_b m_t (\tan \beta + \cot \beta),$$

$$g_{LR} = m_b (\mu + A_b \tan \beta), \tag{A5}$$

$$g_{RL} = m_t (\mu + A_t \cot \beta).$$

APPENDIX B

The form factors F_n^l arise from the renormalized vertices and propagators of the s channel and t channel, as well as from the box diagram given as follows.

The renormalized vertices of s channel:

$$F_1^{V_1(s)} = -3\,\eta_b\{A_{bi}^1 m_{\tilde{g}} p_b \cdot k C_0^1 + A_{bi}^2 m_b[\hat{s} C_0^1 + m_b^2(C_0^1 + 4C_{11}^1 + 2C_{21}^1) + 2p_b \cdot k(C_{11}^1 + 2C_{12}^1 + 2C_{23}^1) - 2m_{\tilde{g}}^2 C_0^1 - 1 + 4C_{24}^1$$

$$+ m_b p_b \cdot k(C_0^1 + C_{11}^1)]\} + \frac{4}{3} A_{bi}^2 \eta_b m_b C_{24}^2 - \frac{16\pi^2}{g_s^2} \eta_t m_b (\delta Z_R^b - \delta Z_L^b),$$

$$F_3^{V_1(s)} = \frac{2}{3}\,\eta_t\{-[m_b^2(C_{11}^1 + C_{21}^1) + p_b \cdot k(C_{12}^1 + C_{23}^1) + C_{24}^1] + A_{bi}^1 m_{\tilde{g}} m_b(C_0^1 + C_{11}^1) + 2A_{bi}^2[C_{24}^1 + p_b \cdot k(C_{12}^1 + C_{23}^1)]\}$$

$$-3\,\eta_t\{[m_b^2(C_0^2 + 2C_{11}^2 + C_{21}^2) + m_{\tilde{g}}^2 C_0^2 - 2C_{24}^2 + 1/2] + 2A_{bi}^1 m_b m_{\tilde{g}}(C_0^2 + C_{11}^2) + 2A_{bi}^2[m_b^2(C_0^2 + 2C_{11}^2 + C_{21}^2)$$

$$- m_{\tilde{g}}^2 C_0^2 - 1/2 + 2C_{24}^2]\} + \frac{16\pi^2}{g_s^2}\,\eta_t 2\,\delta Z_R^b,$$

$$F_7^{V_1(s)} = \frac{1}{3}\,\eta_t(C_{24}^1 - 2A_{bi}^2 C_{24}^1) - \frac{3}{2}\,\eta_t\{m_b^2(C_{21}^2 - C_0^2) + 2p_b \cdot k(C_{12}^2 + C_{23}^2) - m_{\tilde{g}}^2 C_0^2 + 2C_{24}^2 - 1/2 - 2A_{bi}^1 m_b m_{\tilde{g}} C_0^2 \tag{B1}$$

$$- 2A_{bi}^2[m_b^2(C_0^2 + 2C_{11}^2 + C_{21}^2) + 2p_b \cdot k(C_{12}^2 + C_{23}^2) - m_{\tilde{g}}^2 C_0^2 - 1/2 + 2C_{24}^2]\} + \frac{16\pi^2}{g_s^2}\,\eta_t\,\delta Z_R^b,$$

$$F_{2,4,8}^{V_1(s)} = F_{1,3,7}^{V_1(s)}(\eta_t \leftrightarrow \eta_b, A_{bi}^2 \rightarrow -A_{bi}^2, R \leftrightarrow L),$$

$$F_9^{V_1(s)} = \frac{1}{3}\,\eta_b[-m_b(C_{11}^1 + C_{21}^1) + A_{bi}^1 m_{\tilde{g}}(C_0^1 + C_{11}^1) + 2A_{bi}^2 m_b(2C_{12}^1 + 2C_{23}^1 - C_{11}^1 - C_{21}^1)] - 3\,\eta_b[m_b(C_{11}^2 + C_{21}^2)$$

$$+ A_{bi}^1 m_{\tilde{g}} C_{11}^2 + 2A_{bi}^2 m_b(C_{11}^2 + C_{21}^2 - 2C_{12}^2 - 2C_{23}^2)],$$

$$F_{10}^{V_1(s)} = F_9^{V_1(s)}(\eta_b \rightarrow \eta_t, A_{bi}^2 \rightarrow -A_{bi}^2),$$

where the Feynman integrals are defined as $C^1 \equiv C(p_b, k, m_{\tilde{b}_i}, m_{\tilde{g}}, m_{\tilde{g}})$, $C^2 \equiv C(-p_b, -k, m_{\tilde{g}}, m_{\tilde{b}_i}, m_{\tilde{b}_i})$, $C^3 \equiv C(-p_t, -p_{H^-}, m_{\tilde{g}}, m_{\tilde{t}_i}, m_{\tilde{b}_j})$, and

$$F_1^{V_2(s)} = \frac{8}{3}\,\alpha_{ij} A_{ij}^{1R} p_b \cdot k C_{12}^3, \tag{B2}$$

$$F_2^{V_2(s)} = F_1^{V_2(s)}(R \rightarrow L),$$

$$F_3^{V_2(s)} = \frac{8}{3}\,\alpha_{ij}[A_{ij}^{1L} m_b C_{12}^3 + A_{ij}^{1R} m_t(C_{11}^3 - C_{12}^3) - m_{\tilde{g}} A_{ij}^{2L} C_0^3] - \frac{16\pi^2}{g_s^2}\,\eta_t\left[\delta Z_R^t + \delta Z_L^b + 2\frac{\delta m_t}{m_t}\right], \tag{B3}$$

$$F_7^{V_2(s)} = -\frac{4}{3}\,\alpha_{ij}[A_{ij}^{1L} m_b C_{12}^3 + A_{ij}^{1R} m_t(C_{11}^3 - C_{12}^3) - A_{ij}^{2L} m_{\tilde{g}} C_0^3] + \frac{16\pi^2}{g_s^2}\,\eta_t\left[\frac{1}{2}\delta Z_R^t + \frac{1}{2}\delta Z_L^b + \frac{\delta m_t}{m_t}\right],$$

$$F_{4,8}^{V_2(s)} = F_{3,7}^{V_2(s)}\left(R \leftrightarrow L, \eta_t \rightarrow \eta_b, \frac{\delta m_t}{m_t} \rightarrow \frac{\delta m_b}{m_b}\right).$$

Here $A_{(t,b)i}^1 = (-1)^i \sin 2\theta_{t,b}$, $A_{(t,b)i}^2 = \frac{1}{2}(-1)^i \cos 2\theta_{t,b}$. A_{ij} are defined as $A_{ij}^{1L} = 2R_{i2}^t R_{j2}^b$, $A_{ij}^{1R} = 2R_{i1}^t R_{j1}^b$, $A_{ij}^{2L} = -2R_{i2}^t R_{j1}^b$, and $A_{ij}^{2R} = -2R_{i1}^t R_{j2}^b$.

The renormalized vertices of the t channel:

$$F_1^{V_1(t)} = \frac{4}{3} A_{ti}^2 \eta_t m_t C_{24}^4 + 3\,\eta_t\{m_t p_t \cdot k(C_0^5 + C_{11}^5) + A_{ti}^1 m_{\tilde{g}} p_t \cdot k C_0^5 - A_{ti}^2 m_t[\hat{t} C_0^5 + m_t^2(C_0^5 + 4C_{11}^5 + 2C_{21}^5) - 2p_t \cdot k(C_{11}^5 + 2C_{12}^5$$

$$+ 2C_{23}^5) - 2m_{\tilde{g}}^2 C_0^5 - 1 + 4C_{24}^5]\} - \frac{16\pi^2}{g_s^2}\,\eta_t m_t(\delta Z_R^t - \delta Z_L^t),$$

$$F_5^{V_1(t)} = \frac{2}{3}\eta_t\{-[m_t^2(C_{11}^4+C_{21}^4)-p_t\cdot k(C_{12}^4+C_{23}^4)+C_{24}^4]+A_{ti}^1 m_{\tilde{g}}m_t(C_0^4+C_{11}^4)+2A_{ti}^2[-C_{24}^4+p_t\cdot k(C_{12}^4+C_{23}^4)]\}$$

$$-3\eta_t\{m_t^2(C_0^5+2C_{11}^5+C_{21}^5)+m_{\tilde{g}}^2 C_0^5-2C_{24}^5+1/2+2A_{ti}^1 m_t m_{\tilde{g}}(C_0^5+C_{11}^5)-2A_{ti}^2[m_t^2(C_0^5+2C_{11}^5+C_{21}^5)$$

$$-m_{\tilde{g}}^2 C_0^5-1/2+2C_{24}^5]\}-\frac{16\pi^2}{g_s^2}\eta_t 2\,\delta Z_R^t,$$

$$F_7^{V_1(t)} = \frac{1}{3}\eta_t(C_{24}^4+2A_{ti}^2 C_{24}^4)+\frac{3}{2}\eta_t\{m_t^2(C_0^5-C_{21}^5)+2p_t\cdot k(C_{12}^5+C_{23}^5)+m_{\tilde{g}}^2 C_0^5-2C_{24}^5+1/2+2A_{ti}^1 m_t m_{\tilde{g}}C_0^5$$

$$-2A_{ti}^2[m_t^2(C_0^5+2C_{11}^5+C_{21}^5)-2p_t\cdot k(C_{12}^5+C_{23}^5)-m_{\tilde{g}}^2 C_0^5-1/2+2C_{24}^5]\}+\frac{16\pi^2}{g_s^2}\eta_t\delta Z_R^t, \tag{B4}$$

$$F_{2,6,8}^{V_1(t)}=F_{1,5,7}^{V_1(t)}(\eta_t\to\eta_b,A_{ti}^2\to -A_{ti}^2,R\leftrightarrow L),$$

$$F_{11}^{V_1(t)} = \frac{1}{3}\eta_t[m_t(C_{11}^4+C_{21}^4)-A_{ti}^1 m_{\tilde{g}}(C_0^4+C_{11}^4)-2A_{ti}^2 m_t(2C_{12}^4+2C_{23}^4-C_{11}^4-C_{21}^4)]+3\eta_t[m_t(C_{11}^5+C_{21}^5)+A_{ti}^1 m_{\tilde{g}}C_{11}^5$$

$$+A_{ti}^2 2m_t(C_{11}^5+C_{21}^5-2C_{12}^5-2C_{23}^5)],$$

$$F_{12}^{V_1(t)}=F_{11}^{V_1(t)}(\eta_t\to\eta_b,A_{ti}^2\to -A_{bi}^2),$$

where the Feynman integrals are defined as $C^4\equiv C(-p_t,k,m_{\tilde{g}},m_{\tilde{t}_i},m_{\tilde{t}_i})$, $C^5\equiv C(-p_t,k,m_{\tilde{t}_i},m_{\tilde{g}},m_{\tilde{g}})$, $C^6\equiv C(-p_b,p_{H^-},m_{\tilde{g}},m_{\tilde{b}_j},m_{\tilde{t}_i})$, and

$$F_1^{V_2(t)}=-\frac{8}{3}\alpha_{ij}A_{ij}^{1R}p_t\cdot kC_{12}^6,$$

$$F_2^{V_2(t)}=F_1^{V_2(t)}(R\to L),$$

$$F_5^{V_2(t)}=\frac{8}{3}\alpha_{ij}[A_{ij}^{1L}m_b(C_{11}^6-C_{12}^6)+A_{ij}^{1R}m_t C_{12}^6-A_{ij}^{2L}m_{\tilde{g}}C_0^6]-\frac{16\pi^2}{g_s^2}\eta_t\left[\delta Z_R^t+\delta Z_L^b+2\frac{\delta m_t}{m_t}\right], \tag{B5}$$

$$F_7^{V_2(t)}=-\frac{4}{3}\alpha_{ij}[A_{ij}^{1L}m_b(C_{11}^6-C_{12}^6)+A_{ij}^{1R}m_t C_{12}^6-A_{ij}^{2L}m_{\tilde{g}}C_0^6]+\frac{16\pi^2}{g_s^2}\eta_t\left[\frac{1}{2}\delta Z_R^t+\frac{1}{2}\delta Z_L^b+\frac{\delta m_t}{m_t}\right],$$

$$F_{6,8}^{V_2(t)}=F_{5,7}^{V_2(t)}\left(R\leftrightarrow L,\eta_t\to\eta_b,\frac{\delta m_t}{m_t}\to\frac{\delta m_b}{m_b}\right).$$

The renormalized propagators of the s channel:

$$F_1^{s(s)}=\frac{16\pi^2}{g_s^2}\eta_b[2m_b p_b\cdot k(\hat{\Sigma}_L^b+\hat{\Sigma}_S^b)],\qquad F_3^{s(s)}=\frac{16\pi^2}{g_s^2}\eta_t[2(\hat{s}\hat{\Sigma}_L^b+m_b^2\hat{\Sigma}_R^b)+4m_b^2\hat{\Sigma}_S^b],$$

$$\tag{B6}$$

$$F_7^{s(s)}=-\frac{16\pi^2}{g_s^2}\eta_t[\hat{s}\hat{\Sigma}_L^b+m_b^2\hat{\Sigma}_R^b+2m_b^2\hat{\Sigma}_S^b],\qquad F_{2,4,8}^{s(s)}=F_{1,3,7}^{s(s)}(\eta_t\leftrightarrow\eta_b,R\leftrightarrow L).$$

The renormalized propagators of the t channel:

$$F_1^{s(t)} = -\frac{16\pi^2}{g_s^2}\eta_t[2m_t p_t \cdot k(\hat{\Sigma}_L^t + \hat{\Sigma}_S^t)], \qquad F_5^{s(t)} = \frac{16\pi^2}{g_s^2}\eta_t[2(\hat{t}\hat{\Sigma}_R^t + m_t^2\hat{\Sigma}_L^t) + 4m_t^2\hat{\Sigma}_S^t],$$

$$\text{(B7)}$$

$$F_7^{s(t)} = -\frac{16\pi^2}{g_s^2}\eta_t[\hat{t}\hat{\Sigma}_R^t + m_t^2\hat{\Sigma}_L^t + 2m_t^2\hat{\Sigma}_S^t], \qquad F_{2,6,8}^{s(t)} = F_{1,5,7}^{s(t)}(\eta_t \to \eta_b, R \leftrightarrow L).$$

The box diagram contribution:

$$F_1^{box} = \frac{1}{3}\alpha_{ij}A_{ij}^{1R}\left\{9\left[D_{27}^1 + \frac{1}{2}(m_t^2 D_{22}^1 + m_H^2 D_{23}^1) - p_t \cdot k D_{24}^1 + (p_t \cdot k - p_b \cdot k)D_{25}^1 + (p_t \cdot p_b + p_t \cdot k - m_t^2)D_{26}^1\right.\right.$$

$$\left.\left. - p_t \cdot k(D_{12}^1 - D_{13}^1) - \frac{1}{2}m_{\tilde{g}}^2 D_0^1\right] - D_{27}^2\right\},$$

$$F_3^{box} = \frac{1}{3}\alpha_{ij}\{-9[A_{ij}^{1L}m_b D_{23}^1 + A_{ij}^{1R}m_t(D_{23}^1 - D_{26}^1) - A_{ij}^{2L}m_{\tilde{g}}D_{13}^1] + A_{ij}^{1L}m_b(D_{13}^2 - D_{11}^2 - D_{21}^2 - D_{23}^2 + 2D_{25}^2)$$

$$- A_{ij}^{1R}m_t(D_{13}^2 + D_{25}^2 - D_{23}^2) + A_{ij}^{2L}m_{\tilde{g}}(D_0^2 + D_{11}^2 - D_{13}^2)\},$$

$$F_5^{box} = \frac{1}{3}\alpha_{ij}\{9[A_{ij}^{1L}m_b(D_{23}^1 - D_{26}^1) - A_{ij}^{1R}m_t(D_{22}^1 + D_{23}^1 - 2D_{26}^1) + A_{ij}^{2L}m_{\tilde{g}}(D_{12}^1 - D_{13}^1)] + A_{ij}^{1L}m_b(D_{23}^2 - D_{25}^2)$$

$$- A_{ij}^{1R}m_t D_{23}^2 + A_{ij}^{2L}m_{\tilde{g}}D_{13}^2\}, \qquad\qquad\qquad\qquad \text{(B8)}$$

$$F_7^{box} = -\frac{3}{2}\alpha_{ij}[A_{ij}^{1L}m_b D_{13}^1 + A_{ij}^{1R}m_t(D_{12}^1 - D_{13}^1) - A_{ij}^{2L}m_{\tilde{g}}D_0^1],$$

$$F_9^{box} = \frac{1}{3}\alpha_{ij}A_{ij}^{1R}\{-9(D_{23}^1 - D_{25}^1) + D_{13}^2 - D_{12}^2 - D_{24}^2 - D_{23}^2 + D_{25}^2 + D_{26}^2\},$$

$$F_{11}^{box} = \frac{1}{3}\alpha_{ij}A_{ij}^{1R}\{9[D_{12}^1 - D_{13}^1 + D_{23}^1 + D_{24}^1 - D_{25}^1 - D_{26}^1]D_{23}^2 - D_{26}^2\},$$

$$F_{2,4,6,8,10,12}^{box} = F_{1,3,5,7,9,11}^{box}(R \leftrightarrow L),$$

where four-point functions are defined as $D^1 \equiv D(k, -p_t, -p_{H^-}, m_{\tilde{g}}, m_{\tilde{g}}, m_{\tilde{t}_i}, m_{\tilde{b}_j})$, $D^2 \equiv D(-p_b, -k, p_{H^-}, m_{\tilde{g}}, m_{\tilde{b}_j}, m_{\tilde{b}_j}, m_{\tilde{t}_i})$. Note that in the above formulas we take the convention that repeated indices are summed over.

All other form factors F_n^l not listed above vanish. Note that the contributions from diagrams Figs. 1(i), 1(j), and 1(k) just give the renormalization constant δZ_2^g, which is canceled out by δg_s due to the renormalization condition in Eq. (2.4).

The renormalization constants appearing in the above form factors are given by

$$\delta Z_L^t = -\frac{g_s^2 C_F}{16\pi^2}\left\{m_t\left[2m_t\frac{\partial B_1}{\partial p_t^2} - m_{\tilde{g}}A_{ti}^1\frac{\partial B_0}{\partial p_t^2}\right]\right|_{p_t^2 = m_t^2}$$

$$+ (1 - 2A_{ti}^2)B_1\right\}(p_t^2, m_{\tilde{g}}^2, m_{\tilde{t}_i}^2),$$

$$\delta Z_L^b = -\frac{g_s^2 C_F}{16\pi^2}\left\{m_b\left[2m_b\frac{\partial B_1}{\partial p_b^2} - m_{\tilde{g}}A_{bi}^1\frac{\partial B_0}{\partial p_b^2}\right]\right|_{p_b^2 = m_b^2}$$

$$+ (1 - 2A_{bi}^2)B_1\right\}(p_b^2, m_{\tilde{g}}^2, m_{\tilde{b}_i}^2),$$

$$\delta Z_R^t = \delta Z_L^t(A_{ti}^2 \to -A_{ti}^2),$$

$$\text{(B9)}$$

$$\delta Z_R^b = \delta Z_L^b(A_{bi}^2 \to -A_{bi}^2),$$

$$\delta m_t/m_t = \frac{g_s^2 C_F}{16\pi^2}\left(B_1 - \frac{m_{\tilde{g}}}{m_t}A_{ti}^1 B_0\right)(p_t^2, m_{\tilde{g}}^2, m_{\tilde{t}_i}^2),$$

$$\delta m_b/m_b = \frac{g_s^2 C_F}{16\pi^2}\left(B_1 - \frac{m_{\tilde{g}}}{m_b}A_{bi}^1 B_0\right)(p_b^2, m_{\tilde{g}}^2, m_{\tilde{b}_i}^2),$$

where the color factor $C_F = 4/3$, and the renormalized self-energy contributions from quarks are as follows:

$$\hat{\Sigma}_S^t = \frac{g_s^2 C_F}{16\pi^2} \frac{m_{\tilde{g}}}{m_t} A_{ti}^1 [B_0(m_t^2, m_{\tilde{g}}^2, m_{\tilde{t}_i}^2) - B_0(\hat{t}, m_{\tilde{g}}^2, m_{\tilde{t}_i}^2)],$$

$$\hat{\Sigma}_S^b = \frac{g_s^2 C_F}{16\pi^2} \frac{m_{\tilde{g}}}{m_b} A_{bi}^1 [B_0(m_b^2, m_{\tilde{g}}^2, m_{\tilde{b}_i}^2) - B_0(\hat{s}, m_{\tilde{g}}^2, m_{\tilde{b}_i}^2)],$$

$$\hat{\Sigma}_L^t = -\frac{g_s^2 C_F}{16\pi^2}(1 - 2A_{ti}^2)B_1(\hat{t}, m_{\tilde{g}}^2, m_{\tilde{t}_i}^2) - \delta Z_L^t,$$

$$\hat{\Sigma}_L^b = -\frac{g_s^2 C_F}{16\pi^2}(1 - 2A_{ti}^2)B_1(\hat{s}, m_{\tilde{g}}^2, m_{\tilde{b}_i}^2) - \delta Z_L^b,$$

(B10)

$$\hat{\Sigma}_R^t = \hat{\Sigma}_L^t(A_{ti}^2 \to -A_{ti}^2),$$

$$\hat{\Sigma}_R^b = \hat{\Sigma}_L^b(A_{bi}^2 \to -A_{bi}^2).$$

APPENDIX C

In this appendix we give the expansions of the scalar loop integrals in the asymptotic large mass limit. The definitions and conventions of the Feynman loop integral functions can be found in [18]. The integrals are performed in $4 - \epsilon$ dimensions and the divergent contributions are regularized by $\Delta \equiv (2/\epsilon) - \gamma_E + \log(4\pi) - \log(m_h^2/\mu_0^2)$ with m_h being the corresponding mass of the heavy particle in the loops and μ_0 the regularization scale.

Under the assumption of $m_h^2 = \max(m_k^2) \gg p_i \cdot p_j (i,j = 1,2; k = 1,2,3)$, we consider special cases used in our calculations. For the two-point function $B_1(p^2, m_h^2, m_l^2)$, we obtain

$$B_1 = \frac{1}{2}\left\{\Delta + \frac{3 - \delta}{2(1 - \delta)} + \frac{2\delta - \delta^2}{(1 - \delta)^2}\log\delta\right\} + \mathcal{O}\left(\frac{p^2}{m_h^2}\right)$$

(C1)

where $\delta = m_l^2/m_h^2$. Therefore, the asymptotic form can be expressed as

$$B_1 = \begin{cases} \dfrac{\Delta}{2} + \dfrac{p^2}{12m_h^2}, & \delta \to 1, \\[2mm] \dfrac{\Delta}{2} + \dfrac{3}{4} + \dfrac{p^2}{3m_h^2}, & \delta \to 0, \\[2mm] \dfrac{\Delta}{2} + \dfrac{1}{4} + \dfrac{p^2}{6m_h^2}, & \delta \to \infty. \end{cases}$$

(C2)

Note that in the case $\delta \to \infty$ m_h in Eq. (C2) should be replaced by m_l.

For the three-point function $C_{(0,24)}(p_1, p_2, m_1^2, m_2^2, m_3^2)$ we expand them as follows:

Case A. $m_h = m_1$, $m_l^2 = m_2^2 = m_3^2 \pm \Delta_m^2$:

$$C_0 = \frac{1}{m_h^2}\left\{\frac{1}{1 - \delta} + \frac{1}{(1 - \delta)^2}\ln\delta \right.$$
$$+ \frac{p^2}{m_h^2}\left[\frac{\delta + 5}{4(1 - \delta)^3} + \frac{2\delta + 1}{2(1 - \delta)^4}\ln\delta\right]$$
$$\left. + \mathcal{O}\left(\frac{\Delta_m^2}{m_h^2}\right) + \mathcal{O}\left(\frac{p^4}{m_h^4}\right)\right\},$$

(C3)

$$C_{24} = \frac{1}{4}\Delta + \frac{3 - \delta}{8(1 - \delta)} + \frac{2\delta - \delta^2}{4(1 - \delta)^2}\ln\delta$$
$$+ \frac{p^2}{24m_h^2}\left[\frac{2 + 5\delta - \delta^2}{(1 - \delta)^3} + \frac{6\delta}{(1 - \delta)^4}\ln\delta\right]$$
$$+ \mathcal{O}\left(\frac{\Delta_m^2}{m_h^2}\right) + \mathcal{O}\left(\frac{p^4}{m_h^4}\right)$$

where $p = p_1 + p_2$. In the asymptotic large mass limit we obtain

$$C_0 = \begin{cases} -\dfrac{1}{2m_h^2}\left[1 + \dfrac{p^2}{12m_h^2} + \mathcal{O}\left(\dfrac{\Delta_m^2}{m_h^2}\right) + \mathcal{O}\left(\dfrac{p^4}{m_h^4}\right)\right], & \delta \to 1, \\[3mm] \dfrac{1}{m_h^2}\ln\dfrac{m_l^2}{m_h^2}\left[1 + \dfrac{p^2}{2m_h^2} + \mathcal{O}\left(\dfrac{\Delta_m^2}{m_h^2}\right) + \mathcal{O}\left(\dfrac{p^4}{m_h^4}\right)\right], & \delta \to 0. \end{cases}$$

(C4)

$$C_{24} = \begin{cases} \dfrac{1}{4}\Delta + \dfrac{p^2}{48m_h^2} + \mathcal{O}\left(\dfrac{\Delta_m^2}{m_h^2}\right) + \mathcal{O}\left(\dfrac{p^4}{m_h^4}\right), & \delta \to 1, \\[3mm] \dfrac{1}{4}\Delta + \dfrac{3}{8} + \dfrac{p^2}{12m_h^2} + \mathcal{O}\left(\dfrac{\Delta_m^2}{m_h^2}\right) + \mathcal{O}\left(\dfrac{p^4}{m_h^4}\right), & \delta \to 0. \end{cases}$$

(C5)

Case B. $m_l = m_1, m_h = m_2 = m_3$:

$$C_0 = -\frac{1}{m_h^2}\left\{\frac{1}{1-\delta} + \frac{\delta}{(1-\delta)^2}\ln\delta + \frac{p^2}{m_h^2}\left[\frac{1+5\delta}{4(1-\delta)^3} + \frac{\delta^2+2\delta}{2(1-\delta)^4}\ln\delta\right] + \mathcal{O}\left(\frac{p^4}{m_h^4}\right)\right\},$$

(C6)

$$C_{24} = \frac{1}{4}\Delta + \frac{1-3\delta}{8(1-\delta)} - \frac{\delta^2}{4(1-\delta)^2}\ln\delta + \frac{p^2}{24m_h^2}\left[\frac{1-5\delta-2\delta^2}{(1-\delta)^3} - \frac{6\delta^2}{(1-\delta)^4}\ln\delta\right] + \mathcal{O}\left(\frac{p^4}{m_h^4}\right).$$

The asymptotic form is given by

$$C_0 = \begin{cases} -\dfrac{1}{2m_h^2}\left[1 + \dfrac{p^2}{12m_h^2} + \mathcal{O}\left(\dfrac{p^4}{m_h^4}\right)\right], & \delta \to 1, \\[4mm] -\dfrac{1}{m_h^2}\left[1 + \dfrac{p^2}{4m_h^2} + \mathcal{O}\left(\dfrac{p^4}{m_h^4}\right)\right], & \delta \to 0, \end{cases}$$

(C7)

$$C_{24} = \begin{cases} \dfrac{1}{4}\Delta + \dfrac{p^2}{48m_h^2} + \mathcal{O}\left(\dfrac{p^4}{m_h^4}\right), & \delta \to 1, \\[4mm] \dfrac{1}{4}\Delta + \dfrac{1}{8} + \dfrac{p^2}{24m_h^2} + \mathcal{O}\left(\dfrac{p^4}{m_h^4}\right), & \delta \to 0. \end{cases}$$

(C8)

For the four-point functions $D_{0,1k}(p_1, p_2, p_3, m_1^2, m_2^2, m_3^2, m_4^2)$ with the assumption of $m_h^2 = \max(m_k^2) \gg p^2 = \max(p_i \cdot p_j)$ $(i, j = 1,2,3; k = 1,2,3,4)$, we consider two special cases used in our calculations.

Case A. $m_h = m_1, m_l = m_2$:

$$D_0 = \frac{1}{m_h^2 m_l^2}\left\{\frac{1+\delta}{2(1-\delta)^2} + \frac{\delta}{(1-\delta)^3}\ln\delta + \mathcal{O}\left(\frac{\Delta^2}{m_h^2}\right) + \mathcal{O}\left(\frac{p^2}{m_h^2}\right)\right\},$$

(C9)

$$D_{11} = \frac{1}{m_h^2 m_l^2}\left\{\frac{2+5\delta-\delta^2}{4(1-\delta)^3} + \frac{3\delta}{(1-\delta)^4}\ln\delta + \mathcal{O}\left(\frac{\Delta_m^2}{m_h^2}\right) + \mathcal{O}\left(\frac{p^2}{m_h^2}\right)\right\}, \quad D_{12} = \frac{2}{3}D_{11}, \quad D_{13} = \frac{1}{3}D_{11}$$

where $\Delta_m^2 = \max(|m_2^2 - m_3^2|, |m_2^2 - m_4^2|, |m_3^2 - m_4^2|)$. In the asymptotic large mass limit we obtain

$$D_{(0,11,12,13)} = \begin{cases} \left(\dfrac{1}{6}, \dfrac{1}{8}, \dfrac{1}{12}, \dfrac{1}{24}\right)\dfrac{1}{m_h^4}\left[1 + \mathcal{O}\left(\dfrac{p^2}{m_h^2}\right)\right], & \delta \to 1, \\[4mm] \left(\dfrac{1}{2}, \dfrac{1}{2}, \dfrac{1}{3}, \dfrac{1}{6}\right)\dfrac{1}{m_h^2 m_l^2}\left[1 + \mathcal{O}\left(\dfrac{p^2}{m_h^2}\right)\right], & \delta \to 0. \end{cases}$$

(C10)

Case B. $m_h = m_1 = m_2$, $m_l^2 = m_3^2 = m_4^2 \pm \Delta_m^2$:

$$D_0 = -\frac{1}{m_h^4}\left\{ \frac{2}{(1-\delta)^2} + \frac{1+\delta}{(1-\delta)^3}\ln\delta + \mathcal{O}\left(\frac{\Delta_m^2}{m_h^2}\right) + \mathcal{O}\left(\frac{p^2}{m_h^2}\right) \right\},$$

$$D_{11} = \frac{1}{m_h^4}\left\{ \frac{9+3\delta}{4(1-\delta)^3} + \frac{\delta^2-2\delta-2}{2(1-\delta)^4}\ln\delta + \mathcal{O}\left(\frac{\Delta_m^2}{m_h^2}\right) + \mathcal{O}\left(\frac{p^2}{m_h^2}\right) \right\},$$

$$D_{12} = -\frac{1}{m_h^4}\left\{ \frac{5+\delta}{2(1-\delta)^3} + \frac{1+2\delta}{(1-\delta)^4}\ln\delta + \mathcal{O}\left(\frac{\Delta_m^2}{m_h^2}\right) + \mathcal{O}\left(\frac{p^2}{m_h^2}\right) \right\},$$

(C11)

$$D_{13} = \frac{1}{2}D_{12}.$$

In the asymptotic large mass limit we obtain

$$D_{(0,11,12,13)} = \begin{cases} \left(\dfrac{1}{6},\dfrac{1}{8},\dfrac{1}{12},\dfrac{1}{24}\right)\dfrac{1}{m_h^4}\left[1+\mathcal{O}\left(\dfrac{\Delta^2}{m_h^2}\right)+\mathcal{O}\left(\dfrac{p^2}{m_h^2}\right)\right], & \delta\to 1, \\[3ex] \left(-1,-1,-1,-\dfrac{1}{2}\right)\dfrac{1}{m_h^4}\ln\dfrac{m_l^2}{m_h^2}\left[1+\mathcal{O}\left(\dfrac{\Delta_m^2}{m_h^2}\right)+\mathcal{O}\left(\dfrac{p^2}{m_h^2}\right)\right], & \delta\to 0. \end{cases}$$

(C12)

[1] For a review, see, e.g., H.E. Haber and G.L. Kane, Phys. Rep. **117**, 75 (1985).

[2] C.S. Li and J.M. Yang, Phys. Lett. B **315**, 367 (1993); C.S. Li, B.Q. Hu, and J.M. Yang, Phys. Rev. D **47**, 2865 (1993); J.M. Yang, C.S. Li, and B.Q. Hu, *ibid.* **47**, 2872 (1993); J.A. Coarasa *et al.*, Eur. Phys. J. C **2**, 373 (1998).

[3] F. Borzumati, J.-L. Kneur, and N. Polonsky, Phys. Rev. D **60**, 115011 (1999); L.G. Jin, C.S. Li, R.J. Oakes, and Z.-H. Zhu, *ibid.* **62**, 053008 (2000).

[4] S.-H. Zhu, hep-ph/0112109.

[5] A.C. Bawa, C.S. Kim, and A.D. Martion, Z. Phys. C **47**, 75 (1990); V. Barger, R.J. Phillips, and D.P. Roy, Phys. Lett. B **324**, 236 (1994); S. Moretrti and K. Odagiri, Phys. Rev. D **55**, 5627 (1997).

[6] J. Guasch, R.A. Jimenez, and J. Sola, Phys. Lett. B **360**, 47 (1995); R. Jimenez and J. Sola, *ibid.* **389**, 53 (1996); J.A. Coarasa and R.A. Jimenez, *ibid.* **389**, 312 (1996).

[7] For instance, see M. Carena, D. Temes, S. Mrenna, and C.E.M. Wagner, Phys. Rev. D **60**, 075010 (1999); **62**, 055008 (2000); A. Belyaev, D. Garcia, and J. Guasch, *ibid.* **65**, 031701(R) (2002); A. Curiel *et al.*, *ibid.* **65**, 075006 (2002); R.A. Alanakyan and V. Grabski, hep-ph/9711436.

[8] H.E. Haber *et al.*, Phys. Rev. D **63**, 055004 (2001).

[9] M.J. Herrero, S. Peñaranda, and D. Temes, Phys. Rev. D **64**, 115003 (2001).

[10] A. Dobado and M.J. Herrero, Phys. Rev. D **65**, 075023 (2002).

[11] T. Appelquist and J. Carazzone, Phys. Rev. D **11**, 2856 (1975); M. Carena *et al.*, hep-ph/9912516.

[12] CTEQ Collaboration, H.L. Lai *et al.*, Eur. Phys. J. C **12**, 375 (2000).

[13] J.F. Gunion and H.E. Harber, Nucl. Phys. **B272**, 1 (1986).

[14] A. Djouadi, J. Kalinowski, and M. Spira, Comput. Phys. Commun. **108**, 56 (1998).

[15] Mu $g-2$ Collaboration, H.N. Brown *et al.*, Phys. Rev. Lett. **86**, 2227 (2001).

[16] Particle Physics Group, D. Groom *et al.*, Eur. Phys. J. C **15**, 1 (2000), p. 274.

[17] M. Carena, D. Garcia, U. Nierste, and C.E. Wagner, Nucl. Phys. **B577**, 88 (2000); H. Eberl *et al.*, Phys. Rev. D **62**, 055006 (2000).

[18] G. 't Hooft and M. Veltman, Nucl. Phys. **B153**, 365 (1979); G. Passarino and M. Veltman, *ibid.* **B160**, 151 (1979).